NANO LETTERS

pubs.acs.org/NanoLett Letter

Engineering Giant Rabi Splitting via Strong Coupling between Localized and Propagating Plasmon Modes on Metal Surface Lattices: Observation of $\sqrt{N}$ Scaling Rule

Chun-Yuan Wang,[#] Yungang Sang,[#] Xinyue Yang, Soniya S. Raja, Chang-Wei Cheng, Haozhi Li, Yufeng Ding, Shuoyan Sun, Hyeyoung Ahn, Chih-Kang Shih,* Shangjr Gwo,* and Jinwei Shi*

Cite This: *Nano Lett.* 2021, 21, 605−611 Read Online

ACCESS | Metrics & More | Article Recommendations | Supporting Information

ABSTRACT: We present a strong coupling system realized by coupling the localized surface plasmon mode in individual silver nanogrooves and propagating surface plasmon modes launched by periodic nanogroove arrays with varied periodicities on a continuous silver medium. When the propagating modes are in resonance with the localized mode, we observe a $\sqrt{N}$ scaling of Rabi splitting energy, where N is the number of propagating modes coupled to the localized mode. Here, we confirm a giant Rabi splitting on the order of 450−660 meV ($N = 2$) in the visible spectral range, and the corresponding coupling strength is 160−235 meV. In some of the strong coupling cases studied by us, the coupling strength is about 10% of the mode energy, reaching the ultrastrong coupling regime.

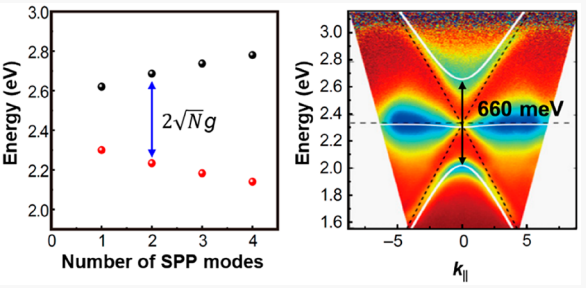

KEYWORDS: *strong coupling, silver surface plasmon lattice, surface plasmon polariton, localized surface plasmon resonance*

Control of light−matter interactions is crucial for the development of photonic science and technology. In the strong coupling regime, the light−matter interaction can lead to the formation of hybridized states (polaritons) with energy shared coherently and reversibly between them.[1−3] Important applications of polaritons have recently been demonstrated, including quantum information processing,[4] quantum many-body phenomena,[5] low-threshold polariton lasers,[6] topological polaritonics,[7,8] and manipulation of chemical reaction landscapes.[9,10] Polariton physics was initially investigated in atomic systems[3] and bulk semiconductors.[11] Subsequently, strong-coupling phenomena have been realized in semiconductor optical cavities via exciton−photon coupling in semiconductor quantum wells,[12] quantum dots[13,14] at cryogenic temperatures, direct- and indirect-exciton in microcavities,[15] and more recently atomically thin van der Waal crystals[16−21] at room temperature. Furthermore, it has been reported that surface periodic structures, such as metal nanoparticle arrays, exhibit surface lattice resonance by diffraction coupling,[22−25] which possess high-density band-edge states[26−28] at high-symmetry points of the surface Brillouin zone. Such kinds of periodic structures in coupling with quantum emitters have the potential to reach the strong coupling regime[29,30] and to realize polariton condensation.[27,31,32] Depending on the coupling strength (g, in units of energy), the energy levels of the polariton states are anticrossed and spectrally separated at resonance by the Rabi splitting (also referred to as the Rabi energy).[1−3] And, it has become obvious that achieving the strong coupling regime with a large Rabi energy will endow great scientific and technological potentials.

For coherent manipulation of the polariton states at room temperature, the Rabi splitting energy must be sufficiently large such that the energy exchange rate in the hybridized system exceeds the light (e.g., cavity photon) and matter (e.g., exciton) decay rates. Especially, in the ultrastrong coupling regime (i.e., the Rabi splitting energy is a significant fraction of the bare energies of the uncoupled systems), novel physical phenomena have been predicted with important implications for quantum optics and quantum computation.[33,34] In this work, we demonstrate a tunable solid-state strong coupling system based on metal metasurfaces[35] involving coupling between localized surface plasmon resonance (LSPR) and propagating surface plasmon modes. As shown in Figure 1a, this system is comprised of deeply trenched ("V"-shaped) nanogrooves with a highly tunable resonance frequency (LSPR mode) and propagating modes, which are Bragg-reflected surface plasmon polariton (SPP) modes folded into the surface Brillouin zone (BZ). Previously, a few experiments have

Received: October 13, 2020
Revised: December 10, 2020
Published: December 22, 2020

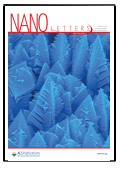

https://dx.doi.org/10.1021/acs.nanolett.0c04099
Nano Lett. 2021, 21, 605−611

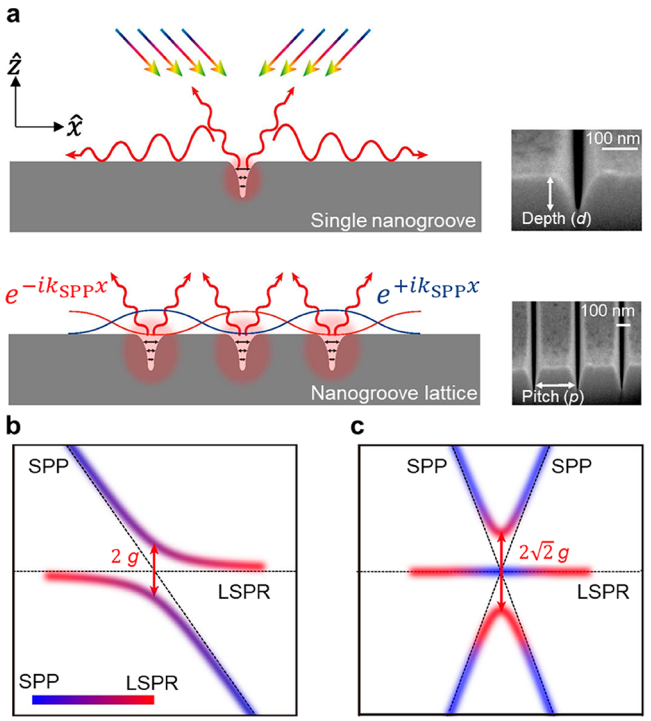

Figure 1. Schematic of strong coupling in the plasmonic nanogroove array. (a) Top: single nanogroove mode exhibiting a dispersionless localized surface plasmon resonance (LSPR) mode excited by resonant light. Bottom: plasmonic nanogroove lattice supporting collective propagation surface plasmon polaritons (SPPs, Bragg-reflected SPP modes). A standing wave can be formed by two SPP modes with opposite propagation directions. When the propagation SPP modes are in resonance with the LSPR, strong coupling between them takes place. Insets: SEM images of focused ion-beam fabricated structures, showing a single nanogroove and a nanogroove lattice. (b) The case of LSPR coupling with one SPP mode, which has a Rabi splitting energy of $2g$. (c) The coherent coupling of LSPR with two SPP modes. The energy splitting of the upper and lower branches is $2\sqrt{2}g$. The color bar shows the hybridization (with different weighting) of LSPR (red) and SPP (blue) modes.

reported coupled systems between localized and propagating modes via nanostructured metal surfaces,[36−40] silicon carbide nanoresonators,[41] and an optical waveguide-plasmon polaritons system.[42,43] Here, we show the experimental evidence for ultrastrong coupling of an all-metal system, allowing for Rabi energy as high as 450−660 meV via patterning nanogroove arrays on a silver continuum. The large coupling strength is due to a $\sqrt{N}$ scaling of Rabi splitting, where N is the number of propagating modes.

The simplest strong coupling scenario occurs when the LSPR mode is coupled to one propagating SPP mode (Figure 1b). In this case, the system can be described by a 2 × 2 Hamiltonian

$$H = \begin{pmatrix} E_{\mathrm{SPP}} - i\gamma_{\mathrm{SPP}}/2 & g \\ g & E_{\mathrm{LSPR}} - i\gamma_{\mathrm{LSPR}}/2 \end{pmatrix} \quad (1)$$

where E_{SPP} and E_{LSPR} represent the energies of SPP and LSPR modes, respectively, γ_{SPP} and γ_{LSPR} denote the decay rates (i.e., full-width at half-maximum (FWHM) line widths of SPP or LSPR modes, resepectively), and g is the coupling strength between them. Under the resonance condition ($E_{\mathrm{SPP}} = E_{\mathrm{LSPR}} = E_0$), the eigenenergies of the coupled system can be solved as the following (complex upper (UB) and lower (LB) branch energies)

$$\tilde{E}_{\mathrm{UB,LB}} = \left(E_0 - i\frac{\gamma_{\mathrm{SPP}} + \gamma_{\mathrm{LSPR}}}{4}\right) \pm \sqrt{g^2 - \frac{(\gamma_{\mathrm{SPP}} - \gamma_{\mathrm{LSPR}})^2}{16}} \quad (2)$$

The strong coupling regime is typically characterized by the real parts of eigenenergies, which have an energy separation $\hbar\Omega_{\mathrm{R}} = 2\sqrt{g^2 - (\gamma_{\mathrm{SPP}} - \gamma_{\mathrm{LSPR}})^2/16}$ that corresponds to the Rabi splitting between two anticrossing energy levels. Furthermore, the two polariton states (i.e., UB and LB) at zero detuning exhibit the same (symmetric) line width, $(\gamma_{\mathrm{SPP}} + \gamma_{\mathrm{LSPR}})/2$, indicating coherent energy exchange and equal mixing of SPP and LSPR modes. To reach the strong coupling regime ($\hbar\Omega_{\mathrm{R}} > 0$), the coupling strength g (proportional to the scalar product of SPP and LSPR vector fields) must be sufficiently large, such that $g > |\gamma_{\mathrm{SPP}} - \gamma_{\mathrm{LSPR}}|/4$. In our design of the localized mode residing in the V-shaped silver nanogroove, as shown in Figure 1a, the strongly enhanced in-plane field in the plasmonic gap mode ensures that the strong coupling condition can be easily fulfilled (g = 160−235 meV in this work).

Due to the small difference in γ_{SPP} and γ_{LSPR} (only a few tens of meV for our structures), we can neglect the damping effects (imaginary parts) and the real eigenenergies can be simplified as the following:

$$E_{\mathrm{UB,LB}} = \frac{E_{\mathrm{SPP}} + E_{\mathrm{LSPR}}}{2} \pm \sqrt{g^2 + \frac{1}{4}(E_{\mathrm{SPP}} - E_{\mathrm{LSPR}})^2} \quad (3)$$

When $E_{\mathrm{SPP}} = E_{\mathrm{LSPR}}$ (i.e., zero detuning), the Rabi splitting energy is $\hbar\Omega_{\mathrm{R}} = 2g$. Considering the nearly linear dispersion of propagating modes $E_{\mathrm{SPP}}(k) = \hbar vk$ (v is the velocity of SPP mode) and dispersionless LSPR, eq 3 can also be used to describe the anticrossing behavior of upper and lower polariton bands (Figure 1b) which has been observed previously.[12−14,18−21]

The more interesting scenario occurs when the LSPR is coupled to two counter-propagating SPP modes (Figure 1c), i.e., N = 2. In this case the Hamiltonian is a 3 × 3 matrix

$$H = \begin{pmatrix} E_{\mathrm{SPP1}} - i\gamma_{\mathrm{SPP1}}/2 & g & g_{\mathrm{SPP-SPP}} \\ g & E_{\mathrm{LSPR}} - i\gamma_{\mathrm{LSPR}}/2 & g \\ g_{\mathrm{SPP-SPP}} & g & E_{\mathrm{SPP2}} - i\gamma_{\mathrm{SPP2}}/2 \end{pmatrix} \quad (4)$$

where SPP1 and SPP2 represent two propagating SPP modes and $g_{\mathrm{SPP-SPP}}$ is the coupling strength between two SPP modes. As discussed below, we assume the dispersion of SPP located in the light-like region. Hence, the direct SPP−SPP coupling term $g_{\mathrm{SPP-SPP}}$ is much weaker than g, and to a good approximation, one can therefore set $g_{\mathrm{SPP-SPP}} \cong 0$. All the main polaritonic behavior is therefore manifested through g, the SPP−LSPR coupling term. If $E_{\mathrm{SPP1}} = E_{\mathrm{SPP2}} \equiv E_{\mathrm{SPP}}$ (this occurs when two SPP modes intersect at the same plasmon momentum) and the damping effect is ignored, the eigenvalues can be expressed as

https://dx.doi.org/10.1021/acs.nanolett.0c04099
Nano Lett. 2021, 21, 605−611

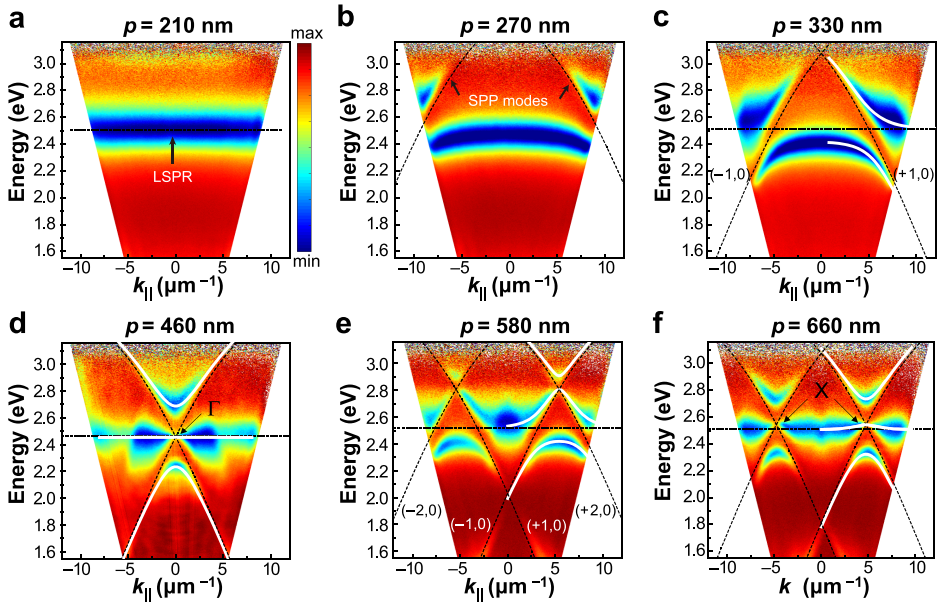

Figure 2. Angle-resolved reflectance spectra in the momentum space. (a–f) The evolution of strong coupling with increasing nanogroove pitch (p) varied from 210 to 660 nm. The complete data set of 17 nanogroove lattices is included in the Supporting Information. The black dashed curves denote the noninteracting LSPR and SPP modes. The white curves are the model fitting results.

$$E_{\mathrm{UB,LB}} = \frac{E_{\mathrm{SPP}} + E_{\mathrm{LSPR}}}{2} \pm \frac{1}{2}\sqrt{(E_{\mathrm{SPP}} - E_{\mathrm{LSPR}})^2 + 8g^2}$$
$$E_{\mathrm{MB}} = E_{\mathrm{SPP}} \tag{5}$$

where MB represents the middle branch. For the case at resonant coupling (i.e., $E_{\mathrm{SPP}} \cong E_{\mathrm{LSPR}}$), the upper and lower polariton branch has a splitting of $2\sqrt{2}g$, which is an enhancement by a factor of $\sqrt{2}$, in comparison with coupling with only one SPP mode. Furthermore, the corresponding eigenstates of the upper, middle, and lower branch can be expressed by the following:

$$\frac{1}{2}\begin{bmatrix}1\\ \sqrt{2}\\ 1\end{bmatrix}_{\mathrm{UB}}, \frac{1}{2}\begin{bmatrix}-\sqrt{2}\\ 0\\ \sqrt{2}\end{bmatrix}_{\mathrm{MB}}, \frac{1}{2}\begin{bmatrix}1\\ \sqrt{2}\\ 1\end{bmatrix}_{\mathrm{LB}} \tag{6}$$

This shows that the spectral weight of LSPR now completely resides at upper and lower branches (represented by the red color shown in Figure 1c). Including the decay rates, the Rabi energy becomes $\sqrt{8g^2 - \frac{1}{4}(\gamma_{\mathrm{SPP}} - \gamma_{\mathrm{LSPR}})^2}$. It is clear that the coupling rate needs to be much higher than the damping rate in order to observe the $\sqrt{2}$ scaling rule. By expanding the Hamiltonian (eq 4) to describe the coupling of the localized mode to N SPP modes, a generalized $\sqrt{N}$ scaling rule can be obtained (see Supporting Information).

Interestingly, the $\sqrt{N}$ scaling behavior of Rabi splitting has a similar form as the behavior of the Jaynes–Cumming (JC) model, describing a quantum emitter being coupled to N photons in a cavity system.[44,45] However, unlike the JC model which is a full quantum description, whose corresponding number N refers to the occupancy number, our system is classical, describing the coupling of a local oscillator to two SPP modes at their zero-occupancy ground state. Moreover, when the two SPP branches are far from resonance with the LSPR mode, their mutual coupling to the LSPR leads to an effective coupling between two SPP modes, even though the direct SPP–SPP coupling is near zero. This can lead to a parabolic SPP band structure, which is shown in Figure S1.

We realized strong coupling experimentally by using a metal metasurface comprised of V-shaped nanogroove arrays on a single-crystalline silver continuum (a large colloidal crystal) with highly tunable LSPR and SPP modes. This system includes three key features to achieve strong and ultrastrong coupling. First, the resonances of both LSPR and SPP modes can be precisely tuned for spectral matching. Second, the SPP propagation modes can be designed to form standing waves with different Bragg reflection orders, whose antinode locations can be tailored to match with the nanogroove locations (mode matching in real space). Third, the SPP propagation modes are nonradiative, leading to less radiative loss and nondiffractive coupling. We note that in previous designs using metal nanoparticle lattices[38−41] or metal nanowire arrays,[42,43] the coupling between the localized mode and the propagating mode is based on diffraction coupling with a limited coupling strength. In our design, the individual nanogrooves act as the plasmonic localized modes with their resonances engineered by tuning the depths and widths of the V-shaped grooves, and the plasmonic gap modes correspond to the Fabry–Pérot resonances along the groove depth direction.[46−48] The localized plasmonic gap mode ensures that the electric field is highly confined within individual grooves.[49,50]

On the other hand, the SPP modes, originating from the Bragg reflections, can be defined by the momentum matching condition as

$$|\mathbf{k}_{\mathrm{SPP}}| = \left|\left(n\frac{2\pi}{p} + k_{\parallel}\right)\hat{\boldsymbol{x}} + \left(m\frac{2\pi}{p}\right)\hat{\boldsymbol{y}}\right| \tag{7}$$

where $\mathbf{k}_{\mathrm{SPP}}$ is the wavevector of the SPP mode on the silver surface, $\hat{x}$ and $\hat{y}$ are in-plane unit vectors perpendicular to and along the groove direction, respectively, $k_{\parallel}$ is the in-plane momentum component of the incident light, p is the lattice

https://dx.doi.org/10.1021/acs.nanolett.0c04099
Nano Lett. 2021, 21, 605−611

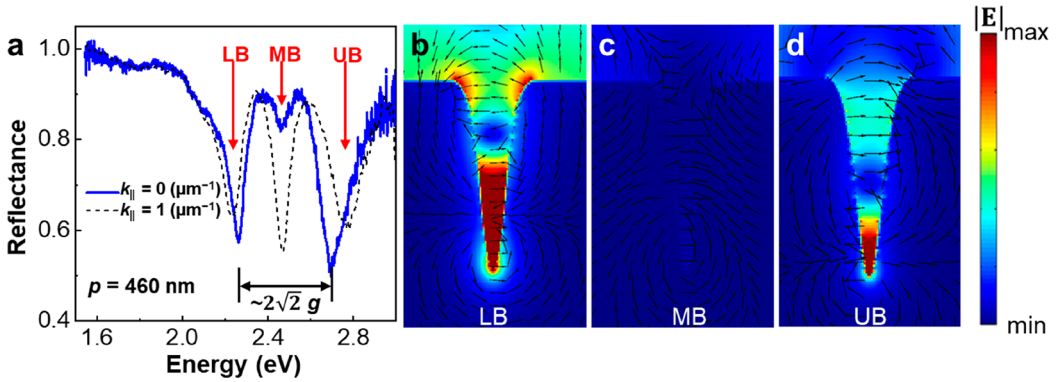

Figure 3. Strong coupling at the Γ point ($k_{\|} = 0$) of the surface Brillouin zone. (a) Reflectance spectrum of the nanogroove lattice with 460 nm pitch (Figure 2d) along two in-plane wavenumbers ($k_{\|} = 0$ and 1 μm^{-1}). An ultralarge quasi-bandgap (Rabi splitting) occurs within a small range of in-plane wavenumber at zero detuning. (b–d) Simulated electric field distributions within the nanogroove on the lower (LB), middle (MB), and upper (UB) branches, respectively, at zero detuning. The coupling parameter for this case is 160 meV. Note that the black arrows of field intensity in (b) and (d) are out of phase, which is a direct illustration of the phase information between UB and LB modes.

period, and (n, m) are the Bragg reflected order. The dispersion curve is a function of lattice period, which means the SPP modes can be tuned to match the LSPR mode in the frequency domain by tuning the lattice period. Here, we adopt the grating direction ($\hat{x}$) and the in-plane momentum of incident light parallel to $\hat{x}$, i.e., m is always zero. Hence, the propagating SPP mode is always along the $\hat{x}$ direction. We note that the direction of $\mathbf{k}_{SPP}$ depends on the Bragg reflection order. When $+\mathbf{k}_{SPP}$ and $-\mathbf{k}_{SPP}$ exist simultaneously at the same energy and at the same $k_{\|}$, the dispersion curves cross with each other in the energy–momentum space, and a standing wave is formed on the surface ($e^{+ik_{SPP}x} + e^{-ik_{SPP}x}$, as shown in Figure 1a). The period of antinodes is always commensurate to the period of the nanogroove array, and the antinodes are located on the nanogrooves, resulting in a strongly enhanced coupling strength.

In our experiments, the LSPR with an eigenenergy E_{LSPR} is independent of k (dispersionless), in contrast to that where the energies of the SPP modes are k dependent. The periodic boundary condition of SPP modes leads to the surface Bloch states, and their energy within the first BZ can be expressed as $E(k)$ (light-like dispersion). Both groove depth (d) and pitch (p) are tuned in this work to optimize the strong coupling conditions. The tuning of lattice parameters is essentially the same as band structure engineering in solid-state physics.[26,51−53] Such kinds of tunability enable us to achieve a greater control in the coupling of LSPR and SPP modes in both momentum and frequency domains (see also Figure S1).

Figure 2 shows a subset of the experimental results (Figure S2 shows our experimental setup). The complete data set of angle-resolved reflectance spectra between LSPR and SPP are shown in the Supporting Information (Figures S3 and S4). The angle-resolved reflectance spectra are transformed to show the dispersion relationship between ω and $k_{\|}$. We control the optical excitation with a transverse magnetic (TM) polarization by using a linear polarizer, and the in-plane incident wavevector is parallel to the grating direction ($\hat{x}$), i.e., the polarization is perpendicular to nanogrooves since the field with parallel polarization to the nanogroove cannot excite the LSPR.[46] Figure 2a shows the bare LSPR mode, which is independent of k. Here, the SPP modes at p = 210 nm within the detectable momentum space (the detectability depends on the numerical aperture of objective) are far from the visible wavelength range. As the pitch is being increased (Figures 2b and 2c), the first-order Bragg reflected SPP modes (±1, 0) start to overlap and couple with the LSPR within the detectable momentum-frequency range and a clear signature of strong coupling between the LSPR and SPP can be observed. The coupling behavior can be fitted by using eq 3. The fitting parameter of coupling strength g shown in the fitted curve of Figure 2c is 180 meV, and the corresponding Rabi splitting energy of experimental data by direct measurement from the image is around 370 ± 5 meV, which is closed to 2g.

When the pitch is increased to 460 nm (Figure 2d), the LSPR is on resonance and coherently coupled to two SPP modes at the same momentum ($k_{\|} = 0$, forming a standing wave), and the energy splitting between upper and lower branches is further enhanced to 455 ± 5 meV. This phenomenon can be characterized by a three-mode coupling described in eq 5 and Figure 1c. Here, we assume the coupling strength ($g_{SPP-SPP}$) between the two SPP modes is zero because of the light-like dispersion. The white lines shown in Figure 2d are the fitted curves with a coupling strength g of 160 meV. We obtain an energy splitting about 1.42 times of 2g, which is very close to $\sqrt{2}$. Note that this coupling strength is 1.6 times stronger than that of the nanowire array structure reported in the literature[42] and satisfies the prediction of the $\sqrt{2}$ scaling rule ($g \gg \frac{1}{4\sqrt{2}}(\gamma_{LSPR} - \gamma_{SPP})$, where $\gamma_{LSPR} \cong 160$ meV and $\gamma_{SPP} \cong 80$ meV). Here, both γ_{LSPR} and γ_{SPP} are extracted from experimental data and the pitch-dependent γ_{LSPR} value. The γ_{LSPR} value of 80 meV used for this estimation is obtained from Figure 2c. For the γ_{SPP} value, the line width of SPP can be extracted through two-mode and three-mode coupling cases at zero detuning, as shown in Figures 3 and 4.

The two polariton branches at the Γ point ($k_{\|} = 0$) have a value of d^2E/dk^2 = 65 meV μm^2 ($\frac{d^2E}{dk^2} = \frac{\hbar^2}{m^*}$), corresponding to an effective mass $m^* = 1.2 \times 10^{-6}$ m_e, where m_e is the free electron mass. In the experimental results shown in Figure 2 (Figure S4), we fix the groove depth/width to keep a constant energy for the LSPR mode. In these cases, the coupling strength g remains nearly constant in the range of 160 to 180 meV. Such a large coupling strength is already enough to observe the -$\sqrt{2}$ scaling rule. In a separate experiment using different groove depth/width values, we can even achieve a Rabi energy of 660 meV with a larger coupling strength (235 meV), and their ratio is also close to 2 $\sqrt{2}$ (shown in the Table

https://dx.doi.org/10.1021/acs.nanolett.0c04099
Nano Lett. 2021, 21, 605−611

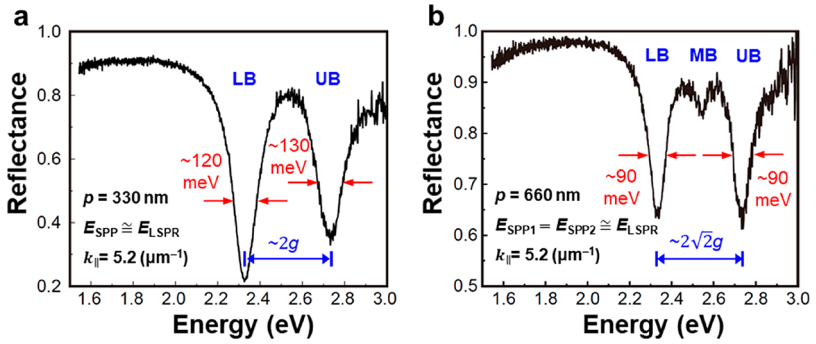

Figure 4. Line widths of strongly coupled modes at zero detuning. (a) Reflectance spectrum of two-mode coupling extracted from Figure 2c along $k_{\parallel} = 5.2\ \mu m^{-1}$. The line widths of LB and UB polations are about the same (120−130 meV) due to hybridization of localized and propagation modes. (b) Reflectance spectrum of three-mode coupling extracted from Figure 2f along $k_{\parallel} = 5.2\ \mu m^{-1}$ (at the X point). The line widths of LB and UB polaritons are about the same.

of Contents image). By further increasing the pitch distance (Figures 2e and 2f), the second order of Bragg-reflected SPP modes start to couple with the LSPR. Due to the mirror symmetry about the Γ point, we can also use the three-mode coupling model to fit the experimental data. For the case of p = 660 nm, the LSPR mode again coherently couples with two SPP modes but at the BZ boundary (X point). This behavior is the same as in Figure 2d with a 1.40 enhancement factor (close to $\sqrt{2}$). It should be noted that the $\sqrt{N}$ scaling rule has also been described in other plasmonic coupling systems.[54] However, there is an essential difference between these two cases. In ref 54 the integer N represents the emitter number or concentration, which is different from the mode number considered here. Another interesting scenario occurs when the SPP modes are far from resonance with the LSPR (Figure 2e). In this case the LSPR acts as a mediator which induces apparent interactions between otherwise noninteracting SPP modes, forming a parabolic SPP band structure with a finite effective mass. It can be demonstrated in the three-mode coupling fitting (eq 5) even when $g_{SPP-SPP} = 0$ (see fitting curves shown in Figure 2e). Here, the parabolic SPP band structures above and below the gap have a finite value of $d^2E/dk^2 = \pm 108$ meV μm^2 (i.e., $m^* = \pm 7 \times 10^{-7}\ m_e$), respectively.

To illustrate the hybridization effects, Figure 3a shows the intensity profile of these three branches as a function of energy at $k_{\parallel} = 0$ and 1 μm^{-1}, respectively (extracted from Figure 2d). The depths of reflectance dips (i.e., absorption peaks) indicate the spectral weighting ratio of LSPR and SPP modes. At $k_{\parallel} = 0$ (LSPR and SPP modes are on resonance), most of the polariton energy is located at upper and lower branches, consistent with the prediction by using eq 6. It can be interpreted as the localized plasmon energy transferring to upper and lower branches, resulting in the formation of a quasi-bandgap. Figures 3b, 3c, and 3d show the simulation results of the near-field distributions on the lower, middle, and upper branches, respectively. These simulations confirm that the energy of LSPR is transferred to the upper and lower branches and that the electric field intensity within the nanogroove is very weak on the middle branch (more detailed simulation spectra can be found in Figure S5). In comparison, at $k_{\parallel} = 1\ \mu m^{-1}$ ($E_{LSPR} \neq E_{SPP}$, close but not exactly on resonance), all three modes contain significant spectral weight of LSPR, resulting in three strong reflectance dips.

The formation of polariton states can be further examined by analyzing the line widths of strongly coupled modes at zero detuning. Figure 4a shows the reflectance spectrum of two-mode (LSPR−SPP) coupling extracted from Figure 2c. The line widths of LB and UB are about the same (120−130 meV) due to hybridization of localized and propagation modes with almost equal spectral weighting (the detuning is only slightly different from zero), and they are consistent with the predicted line width $(\gamma_{SPP} + \gamma_{LSPR})/2$, where $\gamma_{LSPR} \cong 160$ meV and $\gamma_{SPP} \cong 80$ meV. In Figure 4b, we show the reflectance spectrum of three-mode coupling (LSPR−SPP−SPP) at the X point of BZ, which is extracted from Figure 2f along $k_{\parallel} = 5.2\ \mu m^{-1}$. In this case, the line widths of LB and UB are exactly the same (90 meV), in good agreement with the prediction of eq 6.

In summary, we have studied strong coupling of localized plasmonic mode with two propagating SPP modes. We confirm that, when the localized plasmonic mode is resonantly coupled to two SPP modes, the Rabi splitting can be enhanced by a factor of $\sqrt{2}$. Furthermore, noninteracting SPP modes can be manipulated through the localized (on- or off-resonance) plasmonic mode acting as the mediator, which can lead to SPP band structure engineering. For the upper and lower polariton branches, the finite effective masses at the band edges range from 10^{-7} to $10^{-6}\ m_e$. This occurs when the LSPR is coupled with two intersecting SPP modes either resonantly or far from resonance. The effective mass is a major parameter for the realization of Bose−Einstein condensation (BEC) in surface plasmonic lattices.[27,31] A smaller effective mass can lead to a longer thermal de Broglie wavelength and a higher BEC temperature. The effective masses in our experiments are ∼10 to 100 times lighter than that of exciton polaritons[5] and have the same order of magnitude, in comparison with plasmon−exciton polaritons,[27,31] which is based on exciton coupling with the surface plasmon lattice mode, instead of the LSPR−SPP coupling. Therefore, the strong coupling system reported here can potentially open new pathways to study the BEC phenomena on a two-dimensional platform using a simple metallic system with complete tunability.

■ ASSOCIATED CONTENT

Supporting Information

The Supporting Information is available free of charge at https://pubs.acs.org/doi/10.1021/acs.nanolett.0c04099.

Material and methods, metallic nanogroove array fabrication, numerical Rabi splitting simulations by varying the number of SPP modes, additional experimental data, and simulated spectra of LSPR-SPP coupling system (PDF)

https://dx.doi.org/10.1021/acs.nanolett.0c04099
Nano Lett. 2021, 21, 605−611

AUTHOR INFORMATION

Corresponding Authors

Jinwei Shi − *Department of Physics and Applied Optics Beijing Area Major Laboratory, Beijing Normal University, Beijing 100875, China*; Email: shijinwei@bnu.edu.cn

Chih-Kang Shih − *Department of Physics, The University of Texas at Austin, Austin, Texas 78712, United States; Department of Physics, National Tsing-Hua University, Hsinchu 30013, Taiwan;* orcid.org/0000-0003-2734-7023; Email: shih@physics.utexas.edu

Shangjr Gwo − *Department of Physics, National Tsing-Hua University, Hsinchu 30013, Taiwan; Research Center for Applied Sciences, Academia Sinica, Nankang, Taipei 11529, Taiwan;* orcid.org/0000-0002-3013-0477; Email: gwo@phys.nthu.edu.tw

Authors

Chun-Yuan Wang − *Department of Physics, The University of Texas at Austin, Austin, Texas 78712, United States; Department of Physics, National Tsing-Hua University, Hsinchu 30013, Taiwan; Research Center for Applied Sciences, Academia Sinica, Nankang, Taipei 11529, Taiwan*

Yungang Sang − *Department of Physics and Applied Optics Beijing Area Major Laboratory, Beijing Normal University, Beijing 100875, China*

Xinyue Yang − *Department of Physics and Applied Optics Beijing Area Major Laboratory, Beijing Normal University, Beijing 100875, China*

Soniya S. Raja − *Department of Physics, National Tsing-Hua University, Hsinchu 30013, Taiwan*

Chang-Wei Cheng − *Department of Physics, National Tsing-Hua University, Hsinchu 30013, Taiwan*

Haozhi Li − *Department of Physics and Applied Optics Beijing Area Major Laboratory, Beijing Normal University, Beijing 100875, China*

Yufeng Ding − *Department of Physics and Applied Optics Beijing Area Major Laboratory, Beijing Normal University, Beijing 100875, China*

Shuoyan Sun − *Department of Physics and Applied Optics Beijing Area Major Laboratory, Beijing Normal University, Beijing 100875, China*

Hyeyoung Ahn − *Department of Photonics, National Chiao-Tung University, Hsinchu 30010, Taiwan;* orcid.org/0000-0003-3209-6724

Complete contact information is available at: https://pubs.acs.org/10.1021/acs.nanolett.0c04099

Author Contributions

[#]C.-Y.W. and Y.S. contributed equally to this work.

Notes

The authors declare no competing financial interest.

ACKNOWLEDGMENTS

We acknowledge the funding support from the Welch Foundation (F-1672), the Air Force (FA2386-18-1-4097), and the NSF (DMR-1808751) in the United States and MOST (109-2123-M-007-001, 107-2923-M-007-004-MY3) in Taiwan. J.S. acknowledges the support from the NSF of China (91950108, 11774035, 11674032). C.K.S. is thankful for the visiting professorship supported by the Yushan Scholar program of MOE in Taiwan.

REFERENCES

(1) Rabi, I. I. On the process of space quantization. *Phys. Rev.* **1936**, *49*, 324−328.

(2) Rabi, I. I. Space quantization in a gyrating magnetic field. *Phys. Rev.* **1937**, *51*, 652−654.

(3) Allen, L.; Eberly, J. H. *Optical Resonance and Two-level Atoms*; Dover: New York, 1987.

(4) Raimond, J. M.; Brune, M.; Haroche, S. Manipulating quantum entanglement with atoms and photons in a cavity. *Rev. Mod. Phys.* **2001**, *73*, 565−582.

(5) Deng, H.; Haug, H.; Yamamoto, Y. Exciton-polariton Bose−Einstein condensation. *Rev. Mod. Phys.* **2010**, *82*, 1489−1537.

(6) Fraser, M. D.; Höfling, S.; Yamamoto, Y. Physics and applications of exciton-polariton lasers. *Nat. Mater.* **2016**, *15*, 1049−1052.

(7) Karzig, T.; Bardyn, C.-E.; Lindner, N. H.; Refael, G. Topological polaritons. *Phys. Rev. X* **2015**, *5*, 031001.

(8) Klembt, S.; Harder, T. H.; Egorov, O. A.; Winkler, K.; Ge, R.; Bandres, M. A.; Emmerling, M.; Worschech, L.; Liew, T. C. H.; Segev, M.; Schneider, C.; Höfling, S. Exciton-polariton topological insulator. *Nature* **2018**, *562*, 552−556.

(9) Ebbesen, T. W. Hybrid light-matter states in a molecular and material science perspective. *Acc. Chem. Res.* **2016**, *49*, 2403−2412.

(10) Shi, X.; Ueno, K.; Oshikiri, T.; Sun, Q.; Sasaki, K.; Misawa, H. Enhanced water splitting under modal strong coupling conditions. *Nat. Nanotechnol.* **2018**, *13*, 953−958.

(11) Hopfield, J. J. Theory of the contribution of excitons to the complex cielectric constant of crystals. *Phys. Rev.* **1958**, *112*, 1555−1567.

(12) Weisbuch, C.; Nishioka, M.; Ishikawa, A.; Arakawa, Y. Observation of the coupled exciton-photon mode splitting in a semiconductor quantum microcavity. *Phys. Rev. Lett.* **1992**, *69*, 3314−3317.

(13) Reithmaier, J. P.; Sek, G.; Löffler, A.; Hofmann, C.; Kuhn, S.; Reitzenstein, S.; Keldysh, L. V.; Kulakovskii, V. D.; Reinecke, T. L.; Forchel, A. Strong coupling in a single quantum dot-semiconductor microcavity system. *Nature* **2004**, *432*, 197−200.

(14) Yoshie, T.; Scherer, A.; Hendrickson, J.; Khitrova, G.; Gibbs, H. M.; Rupper, G.; Ell, C.; Shchekin, O. B.; Deppe, D. G. Vacuum Rabi splitting with a single quantum dot in a photonic crystal nanocavity. *Nature* **2004**, *432*, 200−203.

(15) Cristofolini, P.; Christmann, G.; Tsintzos, S. I.; Deligeorgis, G.; Konstantinidis, G.; Hatzopoulos, Z.; Savvidis, P. G.; Baumberg, J. J. Coupling quantum tunneling with cavity photons. *Science* **2012**, *336*, 704.

(16) Basov, D. N.; Fogler, M. M.; García de Abajo, F. J. Polaritons in van der Waals materials. *Science* **2016**, *354*, No. aag1992.

(17) Low, T.; Chaves, A.; Caldwell, J. D.; Kumar, A.; Fang, N. X.; Avouris, P.; Heinz, T. F.; Guinea, F.; Martin-Moreno, L.; Koppens, F. Polaritons in layered two-dimensional materials. *Nat. Mater.* **2017**, *16*, 182−194.

(18) Schneider, C.; Glazov, M. M.; Korn, T.; Höfling, S.; Urbaszek, B. Two-dimensional semiconductors in the regime of strong light-matter coupling. *Nat. Commun.* **2018**, *9*, 2695.

(19) Liu, X.; Galfsky, T.; Sun, Z.; Xia, F.; Lin, E.-c.; Lee, Y.-H.; Kéna-Cohen, S.; Menon, V. M. Strong light-matter coupling in two-dimensional atomic crystals. *Nat. Photonics* **2015**, *9*, 30−34.

(20) Liu, X.; Bao, W.; Li, Q.; Ropp, C.; Wang, Y.; Zhang, X. Control of coherently coupled exciton Polaritons in monolayer tungsten disulphide. *Phys. Rev. Lett.* **2017**, *119*, 027403.

(21) Zhang, L.; Gogna, R.; Burg, W.; Tutuc, E.; Deng, H. Photonic-crystal exciton-polaritons in monolayer semiconductors. *Nat. Commun.* **2018**, *9*, 713.

(22) Auguié, B.; Barnes, W. L. Collective resonances in gold nanoparticle arrays. *Phys. Rev. Lett.* **2008**, *101*, 143902.

(23) Kravets, V. G.; Schedin, F.; Grigorenko, A. N. Extremely narrow plasmon resonances based on diffraction coupling of localized plasmons in arrays of metallic nanoparticles. *Phys. Rev. Lett.* **2008**, *101*, 087403.

(24) Zou, S.; Schatz, G. C. Silver nanoparticle array structures that produce giant enhancements in electromagnetic fields. *Chem. Phys. Lett.* **2005**, *403*, 62−67.
(25) Guo, R.; Hakala, T. K.; Törmä, P. Geometry dependence of surface lattice resonances in plasmonic nanoparticle arrays. *Phys. Rev. B: Condens. Matter Mater. Phys.* **2017**, *95*, 155423.
(26) Wang, D.; Yang, A.; Wang, W.; Hua, Y.; Schaller, R. D.; Schatz, G. C.; Odom, T. W. Band-edge engineering for controlled multi-modal nanolasing in plasmonic superlattices. *Nat. Nanotechnol.* **2017**, *12*, 889−894.
(27) Hakala, T. K.; Moilanen, A. J.; Väkeväinen, A. I.; Guo, R.; Martikainen, J.-P.; Daskalakis, K. S.; Rekola, H. T.; Julku, A.; Törmä, P. Bose−Einstein condensation in a plasmonic lattice. *Nat. Phys.* **2018**, *14*, 739−744.
(28) Wang, D.; Bourgeois, M. R.; Lee, W.-K.; Li, R.; Trivedi, D.; Knudson, M. P.; Wang, W.; Schatz, G. C.; Odom, T. W. Stretchable nanolasing from hybrid quadrupole plasmons. *Nano Lett.* **2018**, *18*, 4549−4555.
(29) Yadav, R. K.; Bourgeois, M. R.; Cherqui, C.; Juarez, X. G.; Wang, W.; Odom, T. W.; Schatz, G. C.; Basu, J. K. Room temperature weak-to-strong coupling and the emergence of collective emission from quantum dots coupled to plasmonic arrays. *ACS Nano* **2020**, *14*, 7347−7357.
(30) Sugawara, Y.; Kelf, T. A.; Baumberg, J. J.; Abdelsalam, M. E.; Bartlett, P. N. Strong coupling between localized Plasmons and organic excitons in metal nanovoids. *Phys. Rev. Lett.* **2006**, *97*, 266808.
(31) Rodriguez, S. R. K.; Feist, J.; Verschuuren, M. A.; Garcia Vidal, F. J.; Gómez Rivas, J. Thermalization and cooling of plasmon-exciton polaritons: Towards quantum condensation. *Phys. Rev. Lett.* **2013**, *111*, 166802.
(32) De Giorgi, M.; Ramezani, M.; Todisco, F.; Halpin, A.; Caputo, D.; Fieramosca, A.; Gomez-Rivas, J.; Sanvitto, D. Interaction and coherence of a plasmon-exciton polariton condensate. *ACS Photonics* **2018**, *5*, 3666−3672.
(33) Forn-Díaz, P.; Lamata, L.; Rico, E.; Kono, J.; Solano, E. Ultrastrong coupling regimes of light-matter interaction. *Rev. Mod. Phys.* **2019**, *91*, 025005.
(34) Frisk Kockum, A.; Miranowicz, A.; De Liberato, S.; Savasta, S.; Nori, F. Ultrastrong coupling between light and matter. *Nat. Rev. Phys.* **2019**, *1*, 19−40.
(35) Meinzer, N.; Barnes, W. L.; Hooper, I. R. Plasmonic meta-atoms and metasurfaces. *Nat. Photonics* **2014**, *8*, 889−898.
(36) Kelf, T. A.; Sugawara, Y.; Baumberg, J. J.; Abdelsalam, M.; Bartlett, P. N. Plasmonic band gaps and trapped plasmons on nanostructured metal surfaces. *Phys. Rev. Lett.* **2005**, *95*, 116802.
(37) Teperik, T. V.; Popov, V. V.; García de Abajo, F. J.; Abdelsalam, M.; Bartlett, P. N.; Kelf, T. A.; Sugawara, Y.; Baumberg, J. J. Strong coupling of light to flat metals via a buried nanovoid lattice: the interplay of localized and free plasmons. *Opt. Exp.* **2006**, *14*, 1965−1972.
(38) Yang, J.; Sun, Q.; Ueno, K.; Shi, X.; Oshikiri, T.; Misawa, H.; Gong, Q. Manipulation of the dephasing time by strong coupling between localized and propagating surface plasmon modes. *Nat. Commun.* **2018**, *9*, 4858.
(39) Chu, Y.; Crozier, K. B. Experimental study of the interaction between localized and propagating surface plasmons. *Opt. Lett.* **2009**, *34*, 244−246.
(40) Papanikolaou, N. Optical properties of metallic nanoparticle arrays on a thin metallic film. *Phys. Rev. B: Condens. Matter Mater. Phys.* **2007**, *75*, 235426.
(41) Gubbin, C. R.; Martini, F.; Politi, A.; Maier, S. A.; De Liberato, S. Strong and coherent coupling between localized and propagating phonon polaritons. *Phys. Rev. Lett.* **2016**, *116*, 246402.
(42) Christ, A.; Tikhodeev, S. G.; Gippius, N. A.; Kuhl, J.; Giessen, H. Waveguide-plasmon polaritons: Strong coupling of photonic and electronic resonances in a metallic photonic crystal slab. *Phys. Rev. Lett.* **2003**, *91*, 183901.
(43) Christ, A.; Zentgraf, T.; Tikhodeev, S. G.; Gippius, N. A.; Kuhl, J.; Giessen, H. Controlling the interaction between localized and delocalized surface plasmon modes: Experiment and numerical calculations. *Phys. Rev. B: Condens. Matter Mater. Phys.* **2006**, *74*, 155435.
(44) Meystre, P.; Sargent, M. *Elements of Quantum Optics*; Springer: Berlin, 2013.
(45) Fink, J. M.; Göppl, M.; Baur, M.; Bianchetti, R.; Leek, P. J.; Blais, A.; Wallraff, A. Climbing the Jaynes-Cummings ladder and observing its nonlinearity in a cavity QED system. *Nature* **2008**, *454*, 315−318.
(46) Wang, C.-Y.; Chen, H.-Y.; Sun, L.; Chen, W.-L.; Chang, Y.-M.; Ahn, H.; Li, X.; Gwo, S. Giant colloidal silver crystals for low-loss linear and nonlinear plasmonics. *Nat. Commun.* **2015**, *6*, 7734.
(47) Shi, J.; Liang, W.-Y.; Raja, S. S.; Sang, Y.; Zhang, X.-Q.; Chen, C.-A.; Wang, Y.; Yang, X.; Lee, Y.-H.; Ahn, H.; Gwo, S. Plasmonic enhancement and manipulation of optical nonlinearity in monolayer tungsten disulfide. *Laser Photon. Rev.* **2018**, *12*, 1800188.
(48) Miyazaki, H. T.; Kurokawa, Y. Squeezing visible light waves into a 3-nm-thick and 55-nm-long plasmon cavity. *Phys. Rev. Lett.* **2006**, *96*, 097401.
(49) Volkov, V. S.; Bozhevolnyi, S. I.; Rodrigo, S. G.; Martín-Moreno, L.; García-Vidal, F. J.; Devaux, E.; Ebbesen, T. W. Nanofocusing with Channel Plasmon Polaritons. *Nano Lett.* **2009**, *9*, 1278−1282.
(50) Choo, H.; Kim, M.-K.; Staffaroni, M.; Seok, T. J.; Bokor, J.; Cabrini, S.; Schuck, P. J.; Wu, M. C.; Yablonovitch, E. Nanofocusing in a metal-insulator-metal gap plasmon waveguide with a three-dimensional linear taper. *Nat. Photonics* **2012**, *6*, 838−844.
(51) Kittel, C. *Introduction to Solid State Physics*, 8th ed.; John Wiley and Sons: New York, 2005.
(52) Barnes, W. L.; Preist, T. W.; Kitson, S. C.; Sambles, J. R. Physical origin of photonic energy gaps in the propagation of surface plasmons on gratings. *Phys. Rev. B: Condens. Matter Mater. Phys.* **1996**, *54*, 6227−6244.
(53) Tan, W. C.; Preist, T. W.; Sambles, J. R.; Wanstall, N. P. Flat surface-plasmon-polariton bands and resonant optical absorption on short-pitch metal gratings. *Phys. Rev. B: Condens. Matter Mater. Phys.* **1999**, *59*, 12661−12666.
(54) Törmä, P.; Barnes, W. Strong coupling between surface plasmon polaritons and emitters: a review. *Rep. Prog. Phys.* **2015**, *78*, 013901.

https://dx.doi.org/10.1021/acs.nanolett.0c04099
Nano Lett. 2021, 21, 605−611